A Mechanism for the Effect of Topography on the Martian Hadley Cells

Angela M. Zalucha[1], R. Alan Plumb[1], and R. John Wilson[2], [1]Massachusetts Institute of Technology, 77 Massachusetts Ave. Room 54-1721, Cambridge, MA 02139 (azalucha@mit.edu), [2]Geophysical Fluid Dynamics Laboratory

Introduction

Two recent studies using Mars General Circulation Models (MGCMs) have shown that the north-south slope in the zonally averaged Martian topography produces a Hadley circulation that is asymmetric about the equator. Richardson and Wilson [1] noted in their MGCM results that the annually averaged zonal mean circulation contained a stronger northern hemisphere Hadley cell, which also extended southward across the equator. They performed two further experiments in which the argument of perihelion was shifted by 180° (to test the effect of seasonal differences in the strength of the solar forcing) and in which the zonal mean component of topography was removed (leaving only the mountain or "wave" component). The removal of the zonal mean component of topography created two cells of nearly equal strength and shape, while the shift in the argument of perihelion produced little change from the full MGCM run. These observations suggest that the north-south slope in topography is important, but the strength of the solar forcing is not.

Similarly, Takahashi et al. [2] found that in their MGCM results at equinox, the northern cell was stronger than the southern and extended across the equator into the southern hemisphere. They conducted three runs at perpetual equinox in which variations in only one of the following were included: topography, surface thermal inertia, and surface albedo. The runs with only either surface thermal inertia or surface albedo did not match the control run with all three parameters, but the run with topography did. Two subsequent experiments in which either only the zonal mean component of topography or the zonal wave component were included showed that, as in the study by Richardson and Wilson [1], the zonal mean component of topography is the dominant factor in causing an asymmetric Hadley circulation.

To understand how the surface height affects the atmospheric circulation, we use a simple MGCM, which is thermally forced by Newtonian relaxation to two different radiative equilibrium states, and a modified version of the Hadley cell model of Lindzen and Hou [3], which solves for the boundaries of the cells.

Experiments with a Simple MGCM

We have converted the atmospheric version of the MIT General Circulation Model (GCM) to physical constants appropriate for the Martian atmosphere, which is assumed to be entirely CO_2 and contain no dust. The dynamical core of the MIT GCM solves the fundamental equations of geophysical fluid dynamics in the hydrostatic approximation using the finite volume method on an Arakawa C grid [4]. The horizontal configuration is a cube-sphere grid [5] with 32 × 32 points per cube face, equivalent to a resolution of 2.8° or 166 km at the equator. The vertical grid uses an η coordinate [6] with 30 levels, and the grid spacing increases approximately logarithmically with height. Within each grid point intersecting the surface, the resolution of the topography is increased by inserting sub grids spaced at 10% of the full vertical grid spacing [7]

The external thermal forcing is specified by Newtonian relaxation to a prescribed radiative equilibrium state following Held and Suarez [8]. To the energy equation, the following term is added:

$$\frac{\partial T}{\partial t} = \cdots - k_T \left[T - T_{eq}\right], \tag{1}$$

where T is temperature, t is time, k_T is the radiative relaxation rate (set to 1/2 sols^{-1}), and T_{eq} is the radiative equilibrium temperature, discussed below. Boundary layer friction is specified in the horizontal momentum equations by

$$\frac{\partial v}{\partial t} = \cdots - k_v(p)v, \tag{2}$$

where v is the zonal or meridonal velocity, p is pressure, and k_v is the wind damping rate. k_v is defined by

$$k_v = k_f \max\left(0, \frac{p - p_b}{p_o - p_b}\right), \tag{3}$$

where k_f=1 sol^{-1} is the wind damping rate of the lower atmosphere (as suggested by Held and Suarez [8]), p_o is the surface pressure, and $p_b = 0.7p_o$ is the top of the boundary layer. A similar term to the right side of Eq. 2 is also included in the horizontal momentum equations in the top three model levels (i.e., Rayleigh friction), with k_v set to 9, 3, and 1 sols^{-1} from uppermost to lowermost, respectively.

It should be stressed that T_{eq} is a proxy for the external thermal forcing and does not represent a physical parameter that can be measured. In general, our experiments use two types of radiative equilibrium configura-

tions. The first is referred to as pure radiative equilibrium. Assuming the Eddington approximation, no scattering, no solar absorption by the atmosphere, a gray atmosphere in the long wave, and constant opacity, the solution is

$$\sigma T_{eq}^4 = \begin{cases} Q_o(0.5 + 0.75 p\tau_{oo}/p_{oo}) & p \neq p_o \\ Q_o(1 + 0.75 p_o\tau_{oo}/p_{oo}) & p = p_o, \end{cases} \quad (4)$$

where σ is the Stephan-Boltzmann constant; Q_o is the daily averaged net solar flux, which does not capture diurnal cycles; p_{oo} is a reference pressure, here set to the mean surface pressure of 6 mb; and τ_{oo} is the optical depth at p_{oo}, here taken to be 0.2 to represent non-dusty conditions. Specifically, $Q_o = S_o(1 - A)G$, where S_o is the mean solar constant, A is the albedo (set to a constant value of 0.15), and G is a parameter that depends on orbital characteristics, specifically season (L_s), argument of perihelion, eccentricity, latitude (ϕ), and planetary inclination angle. The seasonal CO_2 cycle is not explicitly included in the model, but T_{eq} and T are snapped back to the frost temperature when they fall below it.

In the pure radiative case defined by Eq. 4, T_{eq} is discontinuous between the surface and the atmosphere directly above the surface. The lapse rate is infinite, which implies an unstable situation. If convection implicitly acts to bring the vertical temperature profile back to the dry adiabatic lapse rate, we arrive at our other radiative equilibrium state, referred to as radiative-convective equilibrium. In radiative convective equilibrium, the temperature above the convective layer is the same as in the pure radiative equilibrium state, and the temperature within the convective layer follows an adiabat. Thus,

$$\sigma T_{eq}^4 = \begin{cases} Q_o(0.5 + 0.75 p\tau_{oo}/p_{oo}) & p < p_t \\ Q_o(0.5 + 0.75 p_t\tau_{oo}/p_{oo})(p/p_t)^{R/c_p} & p \geq p_t, \end{cases} \quad (5)$$

where p_t is the height of the convective layer in pressure coordinates, R is the specific gas constant, and c_p is the specific heat. The height of the convective layer is calculated by setting the net flux (surface plus atmosphere) at the top of the convective layer equal to the net flux at the same level in the pure radiative equilibrium model.

We forced our MGCM with each of the two radiative equilibrium temperatures above (i.e. Eqs. 4 and 5) for the topography measured by the Mars Orbiter Laser Altimeter (MOLA) [9] (hereinafter referred to as full) and full topography with the zonal mean component removed (hereinafter referred to as wave). The MGCM was spun up from an initial rest state with $T = 200$ K everywhere; the time step was 159 s. The season was held fixed at equinox ($L_s = 0$).

Figure 1 shows the results for the zonally averaged mass stream function, time averaged over sols 150 to 180. In the pure radiative equilibrium forcings (top two panels), the Hadley cells are nearly symmetric about the equator, in both strength and the latitude of the streamline dividing the northern and southern cells, for both topographies. For the full topography case, the maximum magnitude of the mass stream function in the northern and southern cells are 4.9 and 3.3×10^8 kg s^{-1}, respectively. The dividing streamline is at the equator near the surface, but has a slight bulge to -5° latitude near 1 mb. For the wave topography case, the maximum magnitude of the mass stream function in the northern and southern cells are 3.3 and 4.8×10^8 kg s^{-1}, respectively. The dividing streamline stays at the equator for all altitudes.

The results with radiative-convective equilibrium forcings (bottom two panels of Fig 1) have a substantial difference between the two topographies. With full topography, the maximum strengths of the northern and southern cells are 17.9 and 4.7×10^8 kg s^{-1}, respectively (c.f. the values from the perpetual equinox run of Takahashi et al. [2] of ~ 35 and $< 5 \times 10^8$ kg s^{-1}, respectively). The latitude of the dividing streamline is at $\sim -15^\circ$ in the lower atmosphere (c.f. $\sim -20^\circ$ from Takahashi et al. [2]). With wave topography, the maximum strengths of the northern and southern cells are 7.8 and 6.0×10^8 kg s^{-1}, respectively (c.f. ~ 7 and $\sim 5 \times 10^8$ kg s^{-1}, respectively, from Takahashi et al. [2]). The dividing streamline is located at the equator, though in Takahashi et al. [2], the northern cell bulges slightly ($\sim 3^\circ$) into the southern hemisphere.

Lindzen and Hou Hadley Cell Model with Topography

Held and Hou [10] created a model that solved for the poleward extent of the Hadley cells assuming symmetric forcing about the equator (i.e. equinox conditions). Their axisymmetric, Boussinesq, hydrostatic model was forced by Newtonian relaxation to a radiative equilibrium state, which was chosen to have a convenient, algebraically simple form. Outside of the Hadley cells, the atmosphere is assumed to be in radiative equilibrium, while the cells themselves are assumed to be momentum conserving. Zonal winds in the Hadley cell region are in cyclostrophic balance, with winds near the ground assumed to be negligable compared with winds near top at the rigid lid boundary (interpreted as the tropopause). There is no net heating within each cell, and temperature is continuous at the latitudinal cell boundaries.

Lindzen and Hou [3] continued the work of Held and Hou [10] by allowing for the maximum solar heating to

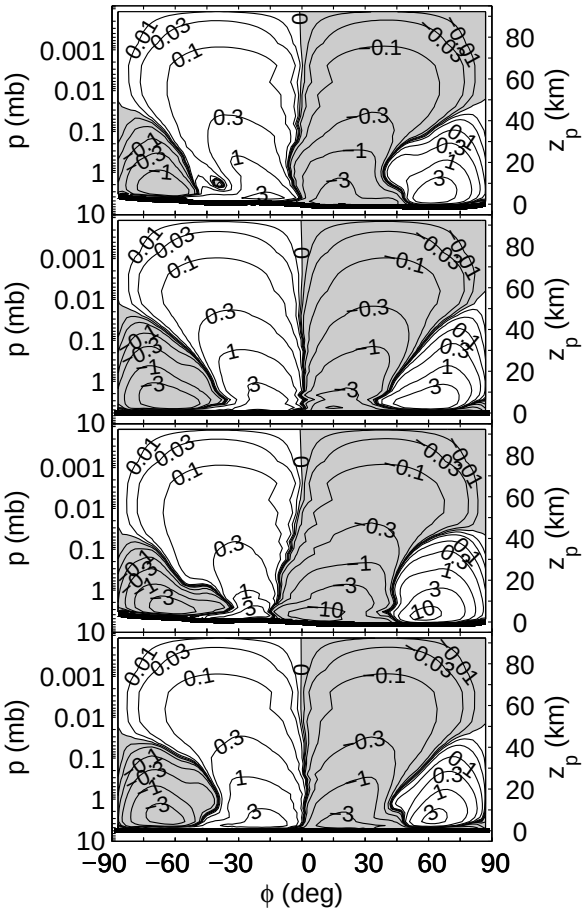

Figure 1: Simple MGCM results for zonally averaged mass stream function (in 10^8 kg s^{-1}), time averaged over sols 150 to 180. From top to bottom, the first panel is full topography forced with pure radiative equilibrium T_{eq}, the second panel is the same as the first but with wave topography (see text), the third panel is full topography forced with radiative-convective equilibrium T_{eq}, and the fourth is the same as the third but with wave topography. Positive is counterclockwise flow; shaded regions indicate negative values. z_p is the approximate geometric height found from $z_p = -h\log(p/p_{oo})$, where $h = 8.5$ km is the scale height.

be centered off the equator. The variables in their model are the latitude of the dividing streamline, ϕ_1, the poleward boundary of the northern cell, ϕ_+, the poleward boundary of the southern cell, ϕ_-, and an integration constant. We have modified their model to allow for a non-zero bottom topography. We also replace their radiative equilibrium state, intended to be for small seasonal

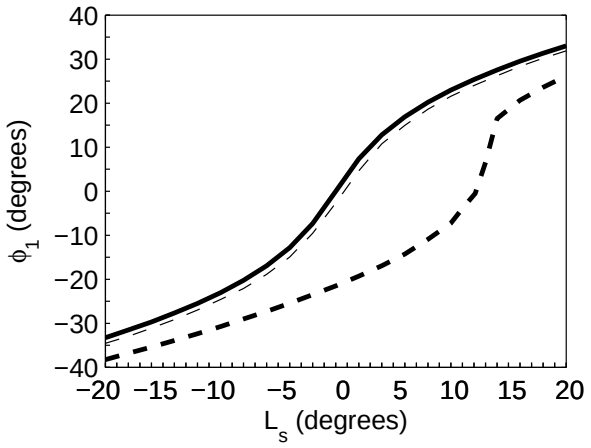

Figure 2: Solution for ϕ_1 from the Lindzen and Hou model with topography. The solid line is the solution for both pure radiative and radiative-convective forcing with flat topography, the thin dashed line is for pure radiative with full topography, and the heavy dashed line is for radiative-convective with full topography.

perturbations to a terrestrial equinoctial state, with the pure radiative equilibrium and radiative-convective equilibrium cases already presented in the previous section (i.e. Eqs. 4 and 5).

Figure 2 shows the solutions for ϕ_1 as a function of L_s for both radiative equilibrium cases with flat topography (since in an axisymmetric model, wave topography is not defined) and full topography. The solution for radiative-convective equilibrium and full topography is clearly offset from the other three. At equinox, ϕ_1 is equal to $-19°$ for this case and $-3°$ for pure radiative equilibrium with topography, and is identically 0 for the two cases without topography. While the solution agrees qualitatively with the MGCM of Takahashi et al. [2] and our MGCM of the previous section, quantitative comparisons are more difficult since the latitude of the dividing streamline in the MGCMs varies with height.

The solutions for ϕ_+ and ϕ_- (not shown) do not agree with our MGCM results, nor do the solutions for ϕ_1 as L_s approaches $\pm 90°$. We are currently performing runs with an axisymmetric version of our MGCM, since it may be more appropriate to compare this configuration to the (axisymmetric) Lindzen and Hou model.

Discussion

Our MGCM and the modified Lindzen and Hou model presented in the preceding two sections qualitatively re-

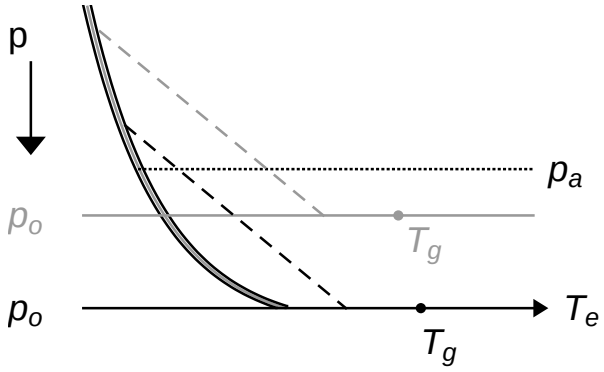

Figure 3: Schematic of the two radiative equilibrium temperature profiles. In radiative-convective equilibrium, the temperature aloft is higher over an elevated surface (gray set of lines) vs. a lower surface (black set of lines), while the temperature aloft does not depend on the height of the surface for the pure radiative equilibrium case (see text for detailed description of symbols).

produce the previously observed behavior of the Hadley cells when forced with a radiative-convective equilibrium state, but not when forced with a pure radiative equilibrium state. Figure 3 shows a schematic of the two radiative equilibrium temperature profiles. First consider the surface described by the solid black line at pressure p_o with pure radiative equilibrium ground temperature T_g (black text) described by the $p = p_o$ case of Eq. 4. The solid gray and black line is the associated pure radiative equilibrium temperature for the atmosphere ($p \neq p_o$). The black dashed line is an adiabat corresponding to radiative-convective equilibrium (the $p \geq p_t$ case of Eq. 5). If the surface is raised to a higher level (lower pressure), now described by the solid gray line, T_g decreases slightly, due to a smaller greenhouse effect, while the pure-radiative equilibrium temperature of the atmosphere remains the same for a given pressure. The gray dashed line is the new adiabat for the higher surface.

If we now consider the temperature aloft at some level p_a (dotted line), the pure radiative equilibrium temperature is the same regardless of the height of the surface. However, the radiative-convective equilibrium temperature is higher above the higher surface. Molnar and Emanuel [11] have also pointed out this effect on a terrestrial model using a more sophisticated radiative transfer algorithm. A thermal forcing that depends on the height of the surface is what allows the surface to communicate with the atmosphere and in turn modify the Hadley circulation.

It is generally accepted that a latitudinal shift in the peak solar heating, such that occurs due to changing season, causes the latitude of the dividing streamline to shift in the same direction, the winter Hadley cell to become stronger, and the summer cell to become weaker. A north-south slope in topography mimics this shift in the peak heating. Because the atmosphere aloft is warmer over an elevated surface, the peak heating shifts towards the higher topography (southward for Mars), as does the dividing streamline. The down slope cell mimics the winter cell (the northern cell for Mars), while the upslope cell mimics the summer cell (the southern cell for Mars).

References

[1] M. I. Richardson and R. J. Wilson. A topographically forced asymmetry in the Martian circulation and climate. *Nature*, 416:298–301, 2002.

[2] Y. O. Takahashi, H. Fujiwara, H. Fukunishi, M. Odaka, Y.-Y. Hayashi, and S. Watanabe. Topographcially induced north-south asymmetry of the meridional circulation in the Martian atmosphere. *J. Geophys. Res.*, 108(E3), 2003. doi: 10.1029/2001JE001638.

[3] R. S. Lindzen and A. Y. Hou. Hadley circulations for zonally averaged heating centered off the equator. *J. Atmos. Sci.*, 45(17):2416–2427, 1988.

[4] J. Marshall, A. Adcroft, C. Hill, L. Perelman, and C. Heisey. A finite-volume, incompressible navier stokes model for studies of the ocean on parallel computers. *J. Geophys. Res.*, 102:5753–5766, 1997.

[5] A. Adcroft, J.-M. Campin, C. Hill, and J. Marshall. Implementation of an atmosphere-ocean general circulation model on the expanded spherical cube. *Mon. Wea. Rev.*, 132:2845–2863, 2004.

[6] A. Adcroft and J.-M. Campin. Rescaled height coordinates for accurate representation of free-surface flows in ocean circulation models. *Ocean Modelling*, 7:269–284, 2004.

[7] A. Adcroft, C. Hill, and J. Marshall. Representation of topography by shaved cells in a height coordinate ocean model. *Mon. Wea. Rev.*, 125:2293, 1997.

[8] I. M. Held and M. J. Suarez. A proposal for the intercomparison of the dynamical cores of atmospheric general circulation models. *Bull. Amer. Meteor. Soc.*, 75(10): 1825–1830, 1994.

[9] D. E. Smith, et al. The global topography of Mars and implications for surface evolution. *Science*, 284(5419): 1495–1503, 1999.

[10] I. M. Held and A. Y. Hou. Nonlinear axially symmetric circulations in a nearly inviscid atmosphere. *J. Atmos. Sci.*, 37:515–533, 1980.

[11] P. Molnar and K. A. Emanuel. Temperature profiles in radiative-convective equilibrium above surfaces at different heights. *J. Geophys. Res.*, 104:24265–24271, 1999.